Pharm Res (2018) 35: 194
https://doi.org/10.1007/s11095-018-2473-7

RESEARCH PAPER

Efficient Nose-to-Lung Aerosol Delivery with an Inline DPI Requiring Low Actuation Air Volume

Dale Farkas[1] • Michael Hindle[2] • P. Worth Longest[1,2]

Received: 18 June 2018 / Accepted: 3 August 2018 / Published online: 21 August 2018

ABSTRACT

Purpose To demonstrate efficient aerosol delivery through an *in vitro* nasal model using a dry powder inhaler (DPI) requiring low actuation air volumes (LV) applied during low-flow nasal cannula (LFNC) therapy.

Methods A previously developed LV-DPI was connected to a LFNC system with 4 mm diameter tubing. System connections and the nasal cannula interface were replaced with streamlined components. To simulate nasal respiration, an *in vitro* nasal model was connected to a downstream lung simulator that produced either passive or deep nasal respiration. Performance of a commercial mesh nebulizer system was also considered.

Results For the optimized system, steady state cannula emitted dose was 75% of the capsule loaded dose. With cyclic nasal breathing, delivery efficiency to the tracheal filter was 53–55% of the loaded dose, which was just under the design target of 60%. Compared with a commercially available mesh nebulizer, the optimal LV-DPI was 40-fold more efficient and 150 times faster in terms of delivering aerosol to the lungs.

Conclusions The optimized LV-DPI system is capable of high efficiency lung delivery of powder aerosols through a challenging nasal cannula interface.

KEY WORDS Dry powder inhaler (DPI) · inline DPI · low flow nasal cannula · low flow oxygen · nasal cannula aerosol · pharmaceutical aerosol

✉ P. Worth Longest
pwlongest@vcu.edu

[1] Department of Mechanical and Nuclear Engineering, Virginia Commonwealth University, 401 West Main Street, P.O. Box 843015 Richmond, Virginia 23284-3015, USA

[2] Department of Pharmaceutics, Virginia Commonwealth University Richmond, Virginia, USA

INTRODUCTION

As previously described (1–6), inline dry powder inhalers (DPI) create a pharmaceutical aerosol in an active manner using a positive pressure gas source external to the recipient. These devices are often advantageous in situations where a subject cannot effectively use a standard oral DPI, such as during most forms of mechanical ventilation, with young children, and when inspiration capacity is limited, as occurs in many respiratory diseases. Compared with jet and mesh nebulizers that are commonly used in these situations, advantages of inline DPIs include rapid dose delivery of an aerosol bolus, the capability to quickly deliver high dose medications, reduced expense and stable drug formulations. The positive pressure gas used to activate the device can also provide a source of respiratory support (1,7). Inline DPIs with high actuation air volumes can open the respiratory airways and control patient breath hold (1,3,7–9), which may be especially important when administering pharmaceutical aerosols to infants and young children. Devices with low actuation air volumes can deliver aerosols very rapidly, which can help to coordinate dose delivery with inhalation and avoids interference with non-invasive ventilation systems allowing for simultaneous therapy (4,5).

Inline DPIs have traditionally been associated with low aerosol delivery efficiency to the lungs (4,10). In more recent publications, new inline DPI systems have been introduced that increase lung delivery efficiency through improved device design and improved formulations. For example, Pornputtapitak *et al.* (2) evaluated the aerosolization of a NanoCluster budesonide formulation with a commercial inhaler in a positive pressure chamber and with a custom inline device. Emitted dose through a 5 mm ID endotracheal tube was approximately 65%, compared to only 15% with a standard commercial budesonide formulation.

With improved delivery devices and formulations, inline DPIs have been tested using *in vitro* experiments for application to invasive mechanical ventilation (3,7), non-invasive positive

pressure ventilation with a face mask (11), and high flow nasal cannula (HFNC) therapy (12). Considering invasive mechanical ventilation, studies by Tang *et al.* (3) and Feng *et al.* (7) have placed the Osmohaler™ containing high dose mannitol powder in a custom chamber and evaluated delivery to the end of endotracheal tubes. Delivery efficiencies using a manual ventilation bag and in a mechanical ventilation system were 50–60% and 25–40%, respectively. The study of Longest *et al.* (8) was the first to consider inline DPI delivery during HFNC therapy. Using a divided cannula that allowed for simultaneous administration and an excipient enhanced growth (EEG) spray dried formulation of ciprofloxacin, <2% of the aerosol was lost in the nose with lung delivery efficiency in the range of 60% of the loaded dose at mean gas flow rates as high as 30 L/min (LPM). More recently, Okuda *et al.* (12) conducted a systematic analysis of an inline Osmohaler™ applied to a HFNC system. Nasal depositional losses were in the range of 50 to 70% and approximately 10–20% of the loaded dose reached a tracheal filter.

Of the different forms of noninvasive respiratory support, low flow nasal cannula (LFNC) oxygen may be the most common. This form of therapy delivers oxygen to the nasal cavity at gas flow rates up to ~8 LPM in adults and ~1 LPM in children to treat hypoxemia (13). With LFNC therapy, the ventilation gas is typically not heated or humidified to maintain system simplicity and the flow rate remains low to avoid nasal discomfort associated with cold temperature and drying. To remain unobtrusive, small diameter tubing and small nasal cannula bore sizes are used, typically with internal diameters (IDs) in the range of 2–4 mm. Patients receiving LFNC therapy and other forms of noninvasive ventilation often require pharmaceutical aerosols for the treatment of underlying lung conditions. Simultaneous administration of a pharmaceutical aerosol through noninvasive ventilation systems and into the lungs (nose-to-lung or N2L delivery) is viewed as convenient and prevents the removal of ventilator support during aerosol delivery (14–16). However, aerosol delivery efficiency through small diameter tubing and cannula systems is known to be very low, with typical values in the range of 0.6–2.5% even at flow rates of 2–5 LPM (17,18).

Our group has recently developed an inline DPI requiring low actuation air volumes (LV) (6) and applied the new LV-DPI to the delivery of pharmaceutical aerosols during LFNC therapy (5). The inline LV-DPI device was operated with an air syringe containing small volumes, typically 10 mL, of room condition air. A custom spacer was developed to integrate the aerosol plume from the LV-DPI into the low velocity gas stream of the LFNC system (5). With the use of the LV-DPI, streamlined connectors and patient interface, and spray dried EEG powder formulations, emitted dose through the small diameter tubing was approximately 65% of loaded dose. Images of the powder exiting the cannula demonstrated a very rapid dose delivery (< 1 s). However, aerosol delivery during realistic *in vitro* testing through a nasal model to the lungs was not evaluated. Furthermore, it has not been determined if actuation of the LV-DPI can be coordinated with cyclic inhalation to enable high efficiency lung delivery of the pharmaceutical aerosol.

The objective of this study was to demonstrate efficient aerosol delivery through an *in vitro* nasal model using a low actuation air volume dry powder inhaler (LV-DPI) system applied during LFNC therapy. Through additional design improvements, lung delivery efficiency in the range of 60% of loaded dose was sought in this highly challenging system. For direct comparison to the use of commercial components, lung delivery efficiency with a mesh nebulizer through the LFNC system and nose-mouth-throat (NMT) model was also evaluated. It is expected that the inline DPI will be significantly more efficient than the commercial system and can be used during cyclic respiration, making this approach an attractive alternative for the administration of high dose or expensive medications such as antibiotics, osmotic agents, surfactants and new anti-inflammatories.

MATERIALS AND METHODS

Materials

Albuterol Sulfate (AS) USP was purchased from Spectrum Chemicals (Gardena, CA) and Pearlitol® PF-Mannitol was donated from Roquette Pharma (Lestrem, France). Poloxamer 188 (Leutrol F68) was donated from BASF Corporation (Florham Park, NJ). L-leucine and all other reagents were purchased from Sigma Chemical Co. (St. Louis, MO). Quali-V, Hydroxypropyl methylcellulose (HPMC) capsules (size 0) were donated from Qualicaps (Whitsett, NC).

Experimental Setup

The experimental setup consisted of a syringe filled with room condition air, the LV-DPI device, spacer, medical grade air (ventilation gas), small diameter Tygon tubing (4 mm ID), streamlined (SL) Y-connector, SL nasal cannula, NMT model and artificial lung simulator (ASL 5000, IngMar Medical, Pittsburgh, PA) or vacuum pump (Fig. 1). As with LFNC therapy, ventilation gas was delivered at a constant flowrate, which in this study was 8 LPM. The nasal cannula was positioned in the nose with a gap between the nasal prongs and nostril to allow for patient exhalation. A downstream vacuum pump or breath simulator was used to create steady state inhalation or cyclic breathing conditions, respectively. To deliver the aerosol, the syringe with 10 mL of room air was actuated by hand as rapidly as possible. High speed video in a previous study (6) indicated that actuation occurs in approximately 0.2 s with minimal resistance felt at the air syringe. Actuating the syringe delivers a bolus of air at approximately 3 LPM through the inline

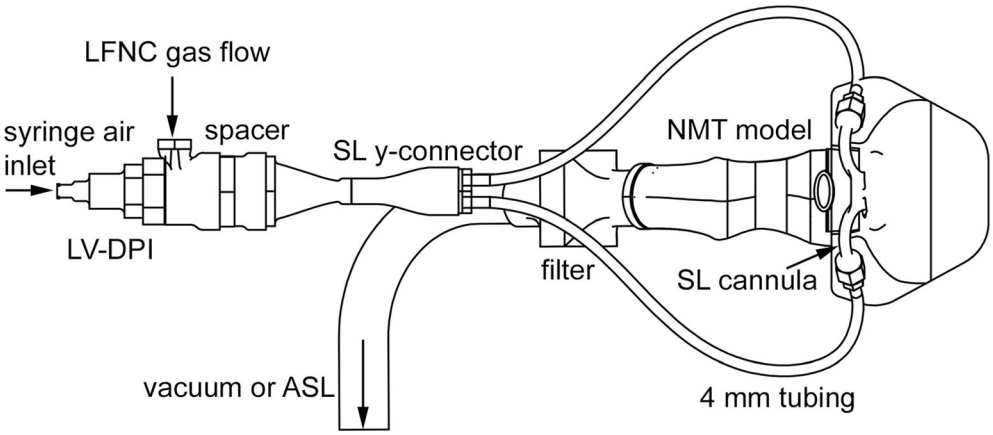

Fig. 1 Schematic of experimental setup showing all major components: LV-DPI, spacer, SL Y-connector, 4 mm tubing, SL cannula, NMT model, filter, LFNC gas flow line, and vacuum/ASL line.

LV-DPI. The spacer is intended to combine the inhaler actuation air with the continuously flowing ventilation gas and produce minimal aerosol loss. Actuation is intended to occur during a period of patient inhalation and deliver all of the aerosol to the patient before exhalation occurs. In this study, steady state inhalation delivery was first considered to assess maximum aerosol delivery efficiency in the absence of exhalation (or respiratory) losses. Experiments with cyclic breathing were then conducted to determine if the aerosol could be effectively delivered during passive and during deep nasal breathing. The mouth was closed in all delivery scenarios. As LFNC systems typically employ tubing with a small bore diameter range of 2 to 4 mm (ID), the larger size of 4 mm medical grade flexible Tygon tubing was selected to minimize aerosol depositional loss.

For comparison to the LV-DPI system explored in this study, experiments were also conducted in a system containing only commercial components. As an inline DPI is not commercially available and use of oral DPIs requires the construction of custom positive pressure enclosures, a commercial mesh nebulizer (Aerogen Solo; Aerogen, Galway, Ireland) was selected. The mesh nebulizer was interfaced with the LFNC delivery line using the commercially available AeroNeb Aerosol Adapter from Vapotherm (Stevensville, MD) which is intended for use with small diameter tubing. The commercial nasal cannula was the Salter Labs 1600TLC (Salter Labs, Arvin, CA). As a minor modification, the supply line for the Salter Labs nasal cannula was shortened to reduce the distance from the outlet of the nebulizer adapter to the Y-connector to improve consistency with the LV-DPI system. Selection of the Salter labs cannula resulted in a tubing ID of 2 mm and a nasal prong ID of 3 mm. The length between the Y-connector and nasal cannula was approximately the same in the two systems considered (450 mm).

LV-DPI and Spacer

The LV-DPI and spacer were previously developed for general applications requiring low actuation air volumes (6) and for specific application to LFNC therapy (5). Briefly, the LV-DPI (Fig. 2a) consists of an inlet sharpened hollow capillary (or capillary set), inhaler body, an outlet sharpened hollow capillary (or capillary set) and a streamlined outlet region. The inhaler body separates in two with a twisting action and a capsule containing the powder is inserted. Closing the inhaler body pierces the capsule and provides a continuous sealed flow path through the device. Air entrained through the inlet capillary forms a turbulent jet that deaggregates the powder. The formed aerosol then enters and flows out of the outlet capillary, where additional deaggregation is expected. The streamlined exit flow passage is intended to contain expansion of the aerosol plume and minimize depositional loss.

The sharpened capillaries are inserted approximately 2 mm into the capsule on both ends, which provides reproducible piercing and high emitted dose (5). The outlet capillary is sharpened on two sides to prevent a capsule flap from interfering with emitted aerosol. The sharpened capillaries are sufficiently recessed in the device to allow for safe operation. This unique device is the only one of which we are aware that combines the steps of closing and piercing in a manner that provides a continuous sealed flow path through the capsule. Use of a size 0 capsule allows for up to 100 mg powder fill mass before powder contacts the capillaries. Based on multiple *in vitro* optimization studies, preferred inlet and outlet capillary diameters are 0.6 mm and 0.89 mm, respectively, for action with 10 mL air pulses and a size 0 capsule (5,6).

The outlet of the LV-DPI leads to a custom spacer that combines the continuously flowing ventilation gas with the aerosol plume. Based on the study of Farkas *et al.* (5), the preferred spacer configuration for LFNC therapy is shown in Fig. 2b and consists of an inlet flow unifier (containing a rod array), mixing region and streamlined outlet. Total volume of the airflow region is 33.7 cm^3, which adds a small amount of travel time to the aerosol moving through the system. The ventilation gas is passed through the flow unifier to generate a constant velocity gas stream that surrounds the inlet aerosol plume. This arrangement is intended to reduce wall deposition and minimize turbulence. The flow unifier consists of multiple rod arrays contained on disks with each disk rotated by 90 degrees forming a 3D mesh. The

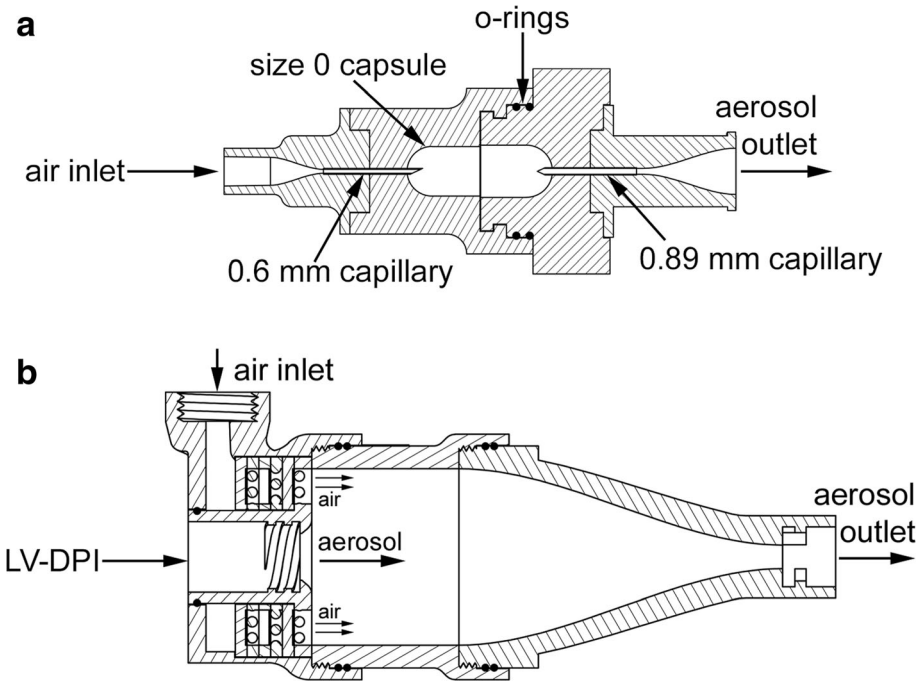

Fig. 2 Section views showing (**a**) LV-DPI device and (**b**) spacer (LV-DPI outlet connects to spacer inlet).

streamlined outlet of the spacer is located sufficiently far from the inlet to reduce impaction losses while maintaining a compact volume and small increase to travel time.

Mesh Nebulizer

The Aerogen Solo mesh nebulizer was selected as a convenient commercially available platform that is often used in ventilation applications. This device was previously used in the *in vitro* study of Perry *et al.* (17), which evaluated aerosol delivery via nasal cannula at different flow rates *in vitro*. The nebulizer formulation for assessing delivery efficiency was 0.5% *w/v* albuterol sulfate (AS) in deionized water. The nebulizer was operated continuously using an Aerogen ProX controller for a period of 90 s, delivering an average nebulized dose of 2.8 mg AS. Based on preliminary experiments, it was determined that the Aerogen Solo produced a MMAD of approximately 5.3 μm from cascade impaction measurements in a humidified environment with a formulation delivery rate of 0.4 mL/min.

Streamlined Components

In the LV-DPI system, a streamlined Y-connector and nasal cannula were employed (Fig. 3). Our group has developed a "streamlined" design concept in which all conduit sudden expansions and contractions are eliminated and direction changes are restricted to a minimum radius of curvature (19–22). This streamlined component approach has previously shown significant increases in aerosol transmission efficiency in both high flow (23) and low flow (19) nose to lung delivery systems. Based on the study of Longest *et al.* (19), an optimized streamlined nasal cannula and Y-connector were implemented in this study as shown in Fig. 3. Both devices utilize 4 mm internal diameter tubing, which is consistent with the 2–4 mm range of commercial LFNC systems. Bayonet style connectors with o-rings were included in the connection components to facilitate assembly and disassembly of an airtight system for determining sectional aerosol deposition. These relatively bulky connectors will not be needed in a final design for clinical use.

Device Preparation

The inhaler body, spacer, Y-connector and streamlined (SL) nasal cannula were created using Autodesk Inventor and exported as STL files to be prototyped. The inhaler and spacer files were then prepared using Objet Studio preparation software and were built using a Stratasys Objet24 3D Printer (Stratasys Ltd., Eden Prairie, MN) using VeroWhitePlus material at a 32 μm resolution. Support material was cleaned away from the model material using a Stratasys waterjet cleaning station and the devices were allowed to fully dry before use. To ensure smooth interior surfaces, the Y-connector and SL nasal cannula were built using stereolithography (SLA) in Accura ClearVue by 3D Systems On Demand Manufacturing (3D Systems Inc., Rock Hill, SC). The capillaries used in the LV-DPIs were custom cut from lengths of stainless steel (SAE 304) capillary tubing and were angled on one side to allow for easy piercing of the capsule upon insertion. O-rings were used as needed to ensure that all components were joined with airtight seals that could withstand the expected operating pressures.

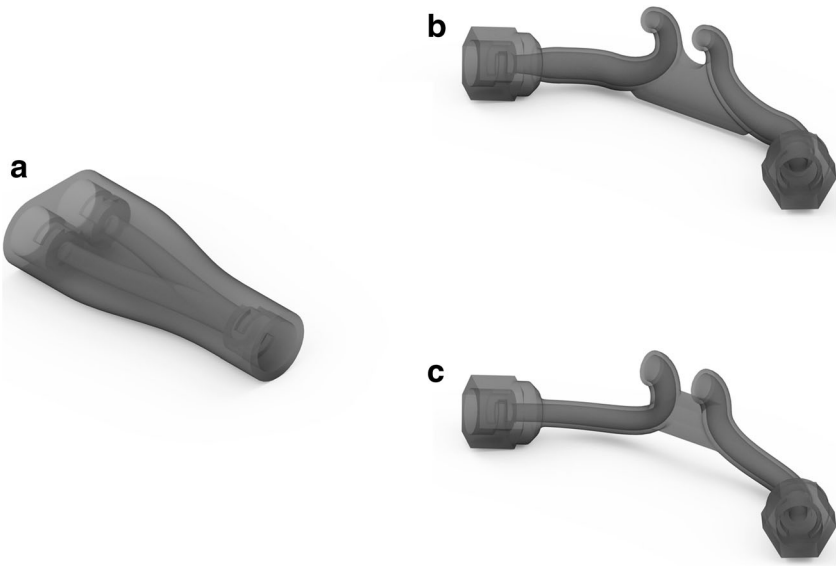

Fig. 3 Images of the streamlined components used in the study: (**a**) Y-connector, (**b**) original cannula (with circular nasal prongs), and (**c**) Cannula 2 (with elliptical nasal prongs).

Airway Models

The airway geometry consisted of a characteristic nose-mouth-throat (NMT) model (shown in Fig. 4) that extended through the larynx. The characteristic NMT model was previously described and implemented in the study of Golshahi *et al.* (24). Briefly, the NMT model included the nasal geometry of Guilmette *et al.* (25), which has been implemented in numerous *in vitro* and numerical studies (26–31). Smoothing of the initial Guilmette *et al.* (25) data was employed to produce a physiologically realistic looking surface. The nasopharynx, pharynx, and larynx were developed from the anatomical CT data used in the previous study of Xi and Longest (32). The oral cavity region was also based on previous CT data and approximates a nearly closed mouth position. Airflow is not included through the mouth opening, consistent with a subject breathing nasally. Based on the study of Walenga *et al.* (11), deposition in this nasal model was similar to deposition in other models over a range of surface area to volume ratios for particle diameters of approximately 1.5 μm. The model was built using Accura ClearVue by 3D Systems On Demand Manufacturing. A filter (Pulmoguard II™, Queset Medical, North Easton, MA) was attached to the exit of the larynx at the tracheal inlet to capture an approximation of the lung delivered dose. The filter outlet was attached to tubing leading to either the vacuum pump or breath simulator.

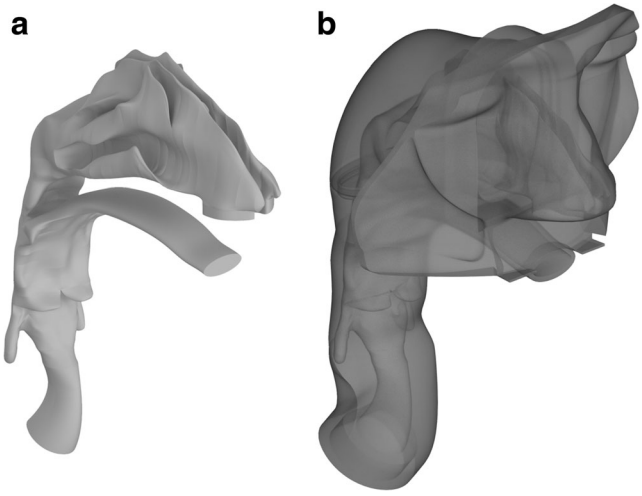

Fig. 4 Images of (**a**) NMT internal geometry and (**b**) NMT external surfaces.

Breathing Conditions

A representative steady state nasal inhalation condition and two different nasal breathing waveforms were considered. To define a passive breathing waveform consistent with a subject sitting awake, respiratory parameters were identified in ICRP (33) with an inspiratory to expiratory time ratio (I:E) of 1:2 (Table I). Assuming sinusoidal inhalation and exhalation waveforms resulted in mean and maximum nasal inhalation flows of 27 and 42.3 LPM, respectively. For deep nasal inhalation during respiratory gas support, *in vivo* data was not available. However, a reasonable set of deep nasal inhalation parameters with ventilation gas was identified in Franca *et al.* (34) for bi-level nasal continuous positive airway pressure. With an I:E ratio of 1:2 and deep nasal inhalation, the resulting mean and maximum nasal inhalation flow rates were 42 and 65.9 LPM, respectively. As the representative steady state flow case, a nasal flow rate of 42 LPM was selected consistent with the mean flow of deep nasal inhalation and maximum flow for passive nasal inhalation.

As shown in Fig. 5, time points t_1 and t_2 define when the constant LFNC ventilation gas plus LV-DPI flow rate (11 LPM) crosses the inhalation waveform. In Table I, $t_{transit}$ is the observed transit time from the start of inhaler actuation to powder

Table I Standard Characteristics for Nasal Inhalation Based on Passive Nasal Inhalation and Deep Nasal Inhalation

Description	Passive nasal	Deep nasal
V_T (L)	0.75	1.75
breaths/min	12	8
I:E	1:2	1:2
T_{inhale} (s)	1.67	2.5
T_{total} (s)	5.0	7.5
Q_{mean} (LPM)	27.0	42.0
Q_{max} (LPM)	42.3	65.9
t_1 [a] (s)	0.14	0.135
t_2 [b] (s)	1.5	2.4
t_2-t_1 [c] (s)	1.36	2.27
$t_{transit}$ [d] (s)	0.2	0.2
t_{exit} [e] (s)	0.5	0.5

a Intersection of breathing flow and HFNC flow rate - rising flow

b Intersection of breathing flow and HFNC flow rate - falling flow

c Time that HFNC flow rate is below breathing flow rate

d Transit time through the LV-DPI + LFNC system between the start of actuation and the first appearance of aerosol from the cannula tip

e Time for the aerosol to exit the LV-DPI and LFNC system from the first to the last appearance of powder from the cannula tip

first exiting the cannula. The time period required for powder to exit the cannula is t_{exit}. For both inhalation cases, it is observed that the system can be actuated at the start of inhalation.

Powder Formulation

A single batch of spray dried albuterol sulfate (AS) EEG formulation was produced using the optimized method described by Son *et al.* (35). The primary particle size of the spray dried batch was determined using a laser diffraction method with a Sympatec ASPIROS dry dispersing unit and HELOS laser diffraction sensor.

Device Improvements

Modifications were made to some components of the LV-DPI system based on observations of depositional losses. The Y-connector originally consisted of a 4 mm diameter inlet which bifurcated into two 4 mm outlets. To match the average velocity of the inlet to that of the two outlets, and thereby reduce depositional losses, the diameter of the inlet was increased to 5.7 mm, which provided the same cross-sectional area as the two combined outlet areas. This increase in diameter also required the outlet of the spacer to be redesigned for the same 5.7 mm diameter, as well as the removal of the small piece of 4 mm diameter tubing that was positioned between the spacer and the Y-connector. The cannula was also redesigned to both decrease retention and lower NMT deposition by changing the outlet cross sections from a circular (diameter = 4 mm) to an elliptical design with a slightly larger cross section. Dimensions of the elliptical cannula outlets were 6 mm tall × 4 mm wide. Specifically, the original cannula was used in the study of Farkas, Hindle and Longest (5) and had characteristic circular outlet prongs. The first cannula revision with elliptical outlet prongs (Cannula 1) maintained a 4 mm diameter through the cannula until the beginning of the nasal prong, which is where the transition to the elliptical outlet began. As a second cannula revision (Cannula 2), elliptical outlet prongs were transitioned immediately beginning at the circular cannula inlet.

Device Operation

Aerosolization performance of the LV-DPIs was characterized using 10 mg of EEG-AS powder formulation, which was accurately weighed and manually filled into size 0 capsules. This 10 mg mass of powder filled approximately 3% of the capsule volume. Loaded capsules were placed in one half of the LV-DPI and pierced when the two device halves were sealed together with a 30° turn. After device assembly, a 10 mL syringe was filled with room air and then connected via the luer-lock onto a 3-way stopcock that was connected to the LV-DPI inlet. The powders were then aerosolized with the LV-DPI in a horizontal position as shown in Fig. 6. As minimal size change is expected in the aerosol under ambient temperature and relative humidity (RH) conditions, experiments were conducted with ambient air ($T = 22 \pm 3$°C and RH = 50 ± 5%). To actuate the LV-DPI, the plunger of the syringe was depressed quickly (~0.2 s to empty) to aerosolize the powder. For experiments using cyclic breathing, the inhaler was actuated at the time point when inhalation began as observed on the breath simulator display (equivalent to watching a patient begin inhaling). After each actuation, the stopcock valve was turned to the off position for the device and the syringe was refilled with room air through the open port for a total of 5 actuations. Syringe emptying times were determined in our previous work using a single operator and high speed photography at 1000 frames/s (6). All measurements were made with three replicates for each design configuration.

Characterization Methods

After aerosolization, drug masses retained in the capsule, device, spacer, system components (tubing, Y-connector and cannula), NMT model and tracheal filter were recovered by washing with appropriate volumes of deionized water and quantified by HPLC analysis. AS quantification was performed with a validated HPLC method using a Waters 2695 separations module with a 2475 fluorescence detector (Waters Co., Milford, MA). Chromatography was performed using a Restek Allure PFP 150 mm × 2.1 mm column (Bellefonte, PA). The mobile phase, consisting of methanol and ammonium

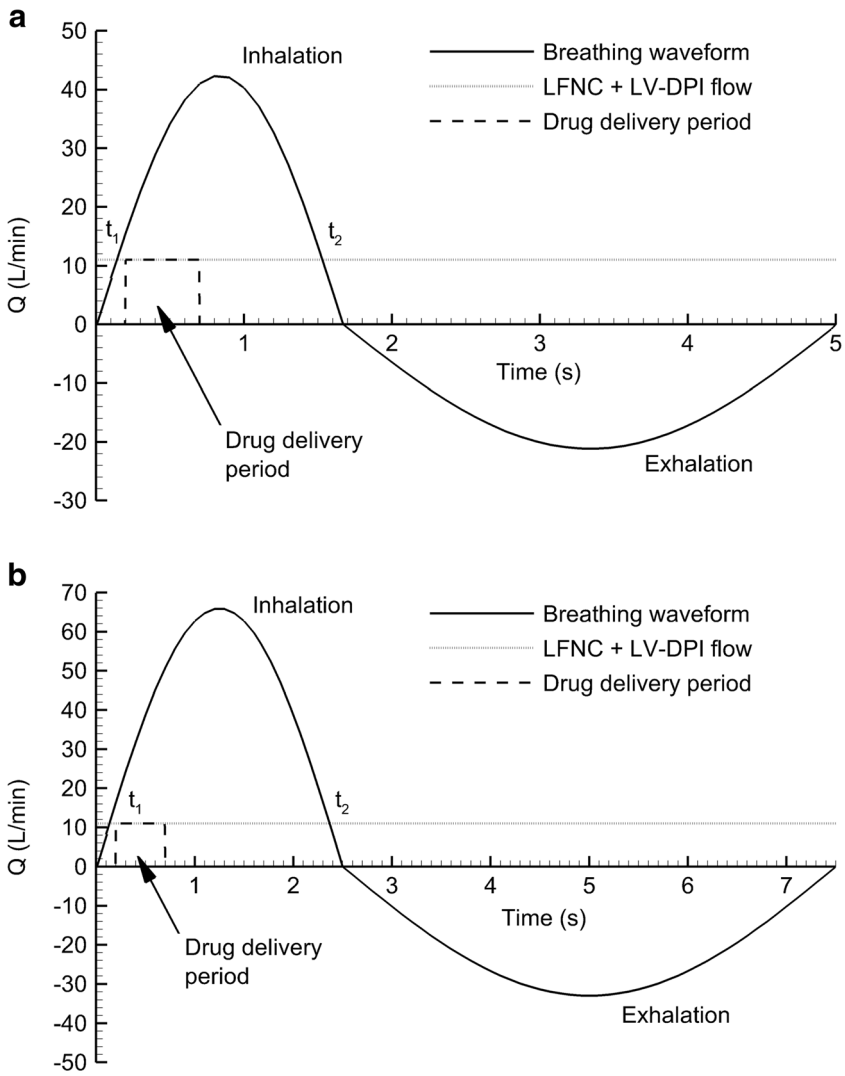

Fig. 5 Graphs showing the two breathing profiles used in this study: (**a**) Passive Nasal inhalation and (**b**) Deep Nasal inhalation.

formate buffer (20 mM, pH 3.4) in a ratio of 70:30, respectively, was eluted at a flow rate of 0.4 mL/min and the detector was set to an excitation wavelength of 276 nm and emission at 609 nm. The column temperature was maintained at 25°C, and the volume of each sample injected was 100 µL. The limit of quantification was 0.5 µg/ml. The mass of AS retained or deposited in each component was expressed as a percentage of the AS dose loaded into each capsule. In order to determine the nominal dose of AS in the EEG-AS formulation, known masses of the formulation were dissolved in 50 mL of water and the mean amount of AS per mg of formulation was determined using the HPLC analysis method. For each aerosolization experiment, the measured formulation AS content and the mass of

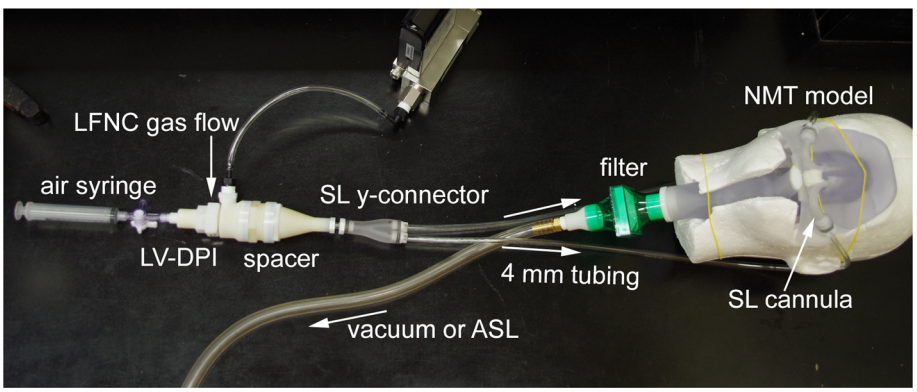

Fig. 6 Picture of experimental setup showing all major components: air syringe, LV-DPI, spacer, SL Y-connector, 4 mm tubing, SL cannula, NMT model, filter, LFNC gas flow line, and vacuum/ASL line.

formulation loaded into the capsule was used to determine the loaded dose of AS.

To determine the emitted dose (ED) of the nebulizer system, the nebulizer was weighed before and after each experiment. Just as with the DPI experiments, each component was then assayed separately to determine the amount of deposited drug. The mass of AS retained in each nebulizer system component was then expressed as a percentage of the ED.

RESULTS

Initial System Evaluation

The same system used in our previous study (5) was first evaluated using the NMT model, which included the spacer with a 4 mm outlet, unmodified Y-connector, and the original cannula. First, a steady state approximation of only inhalation was used to determine the maximum tracheal filter deposition achievable without introducing losses due to exhalation. As shown in Table II, the steady state conditions produced an average filter delivery of 50.9% of the capsule loaded dose. Cyclic breathing with deep nasal and with passive nasal inhalation produced filter deliveries of 46.9 and 46.4%, respectively, which was not statistically different (p-value = 0.171) from the steady state case. To evaluate exhalation losses that may potentially occur with cyclic inhalation, the amount of drug recovered from all system components was provided in Table II as a function of loaded dose. It was observed that the steady state and both breathing profiles produced statistically equivalent recovery values. As a result, it was concluded that the exhalation losses are small for the cyclic breathing conditions. Relatively low deposition (3–6%) in the NMT model was observed in both the steady state and realistic breathing cases. Using components from the previous system (5), it is observed that the filter delivered dose of 46–51% is below the design target of 60%. Hence, modifications to the spacer, Y-connector, and cannula were made and explored below.

Table II Mean (SD) *In Vitro* Aerosol Drug Delivery Using the Original LFNC Delivery Components as Developed in Farkas *et al*. (2018) Applied to the NMT Model Under Steady State Inhalation and Cyclic Breathing Conditions

Description	Steady state	Deep nasal	Passive nasal
Capsule (%)	13.9 (7.5)	17.1 (4.1)	19.6 (5.2)
Device (%)	2.4 (0.2)	3.3 (0.6)	3.1 (0.3)
Device ED (%)	83.7 (7.4)	79.6 (4.3)	77.3 (5.0)
Spacer (%)	6.6 (0.9)	6.1 (0.4)	7.3 (1.5)
Y Retention (%)	4.5 (1.1)	3.6 (0.6)	3.5 (0.9)
Tubing Retention (%)	5.8 (0.8)	4.5 (2.1)	4.5 (2.1)
Cannula Retention (%)	4.9 (2.1)	4.1 (1.4)	3.6 (1.9)
Cannula Emitted (%)	61.9 (2.8)	61.3 (0.8)	58.5 (1.4)
NMT (%)	4.6 (1.5)	6.0 (1.9)	3.6 (1.3)
Filter Delivery (%)	50.9 (3.0)	46.9 (1.0)	46.4 (3.5)
Recovery (%)	93.6 (1.2)	91.6 (3.3)	91.5 (3.9)

Values are reported as a percentage of nominal dose loaded into the capsule. Standard deviations (SD) shown in parenthesis [n = 3]

Modified System Optimization

The modified system was evaluated using steady state conditions and compared to the original system, in order to determine the optimal cannula design (Table III). Modifications included the spacer outlet, Y-connector (Fig. 3a) and cannula selection (Fig. 3b and c). The redesigned Y-connector showed a significant retention decrease from 4.5% (original system) to 0.5% under steady state conditions (Table III). While no other components in the system showed significant decreases compared to the original system, the cannula ED of both cannula designs was found to be significantly higher (69.3 and 74.7% for Cannula 1 and Cannula 2, respectively). Considering delivery to the tracheal filter, Cannula 2 produced a higher value (61.6%) with lower variability (standard deviation (SD) = 4.8%) compared with Cannula 1, and was therefore selected for further consideration in this study.

Using the modified system with the Cannula 2 design, realistic breathing profiles were considered with results reported in Table IV in comparison to the steady state case. Cyclic flow decreased filter delivery to the range of 53–55%; however, these values were not statistically different (p-value = 0.200) from the steady state case of 62%. Recovery values between steady state and breathing conditions again showed that

Table III Comparison of the Mean (SD) *In Vitro* Aerosol Drug Delivery Using the Original Delivery System and the Updated Version, with Two New Cannula Designs, Using Steady State Inhalation Conditions

Description	Original	Cannula 1	Cannula 2
Capsule (%)	13.9 (7.5)	12.8 (1.1)	8.6 (0.5)
Device (%)	2.4 (0.2)	2.3 (0.8)	1.6 (0.4)
Device ED (%)	83.7 (7.4)	85.2 (1.2)	89.8 (0.2)
Spacer (%)	6.6 (0.9)	6.4 (0.4)	6.4 (0.8)
Y Retention (%)*	4.5 (1.1)	0.5 (0.2)**	0.5 (0.1)**
Tubing Retention (%)	x5.8 (0.8)	4.1 (0.9)	4.0 (0.8)
Cannula Retention (%)	4.9 (2.1)	5.0 (1.6)	4.1 (1.2)
Cannula ED (%)*	61.9 (2.8)	69.3 (2.7)**	74.7 (3.0)**
NMT (%)	4.6 (1.5)	7.3 (2.9)	6.9 (2.0)
Filter Delivery (%)	50.9 (3.0)	54.6 (8.5)	61.6 (4.8)
Recovery (%)	93.6 (1.2)	92.6 (3.6)	93.8 (0.7)

Values are reported as a percentage of nominal dose loaded into the capsule. Standard deviations (SD) shown in parenthesis [n = 3]

*$p < 0.05$ significant effect of system design on Y Retention and Cannula ED (one-way ANOVA)

**$p < 0.05$ significant difference compared to Original (post-hoc Tukey)

minimal exhalation loss occurred during administration. While a difference was found in the amount of drug recovered during Passive Breathing, the absolute difference was small (~3%) indicating that exhalation losses are minimal.

Comparison to Continuous Nebulizer Delivery

Regional depositional loss and tracheal filter delivery percentage for the mesh nebulizer system and passive nasal inhalation are provided in Table V. Based on high delivery system losses, the cannula ED is only 15.7%. Due to high depositional losses and selective filtering of the larger droplets, the aerosol exiting the cannula is likely small resulting in negligible NMT deposition (Table V). However, due to continuous nebulization with the commercially available nebulizer, exhalation losses are high leading to only 1.4% of the nebulized dose reaching the tracheal filter.

DISCUSSION

The modified LV-DPI system came very close to achieving the initial design goal of delivering 60% of the loaded drug to the tracheal filter during cyclic breathing. System modifications were shown to increase the cannula ED from 62% to a range of 69–75% during steady state inhalation. However, cyclic nasal breathing and some NMT deposition (<10%) reduced delivery to the tracheal filter from approximately 62% at steady state to a range of 53–55%, which was just below the 60% target. While the design goal was not fully met during transient inhalation, delivery efficiency to the tracheal filter is still high for this very challenging system that includes small diameter tubing (~4 mm ID), cyclic breathing, and uncontrolled electrostatic charge.

Table IV Comparison of Mean (SD) *In Vitro* Aerosol Drug Delivery Using Steady State Performance and Realistic Inhalation Conditions with the Revised Delivery System and Cannula 2

Description	Steady state	Deep nasal	Passive nasal
Capsule (%)	8.6 (0.5)	11.1 (2.6)	9.5 (2.5)
Device (%)	1.6 (0.4)	1.7 (0.4)	1.7 (0.6)
Device ED (%)	89.8 (0.2)	87.2 (2.9)	88.8 (2.9)
Spacer (%)	6.4 (0.8)	7.4 (2.2)	7.3 (1.6)
Y Retention (%)	0.5 (0.1)	0.7 (0.3)	0.7 (0.3)
Tubing Retention (%)	4.0 (0.8)	5.0 (1.8)	4.9 (1.4)
Cannula Retention (%)	4.1 (1.2)	4.7 (1.9)	4.6 (1.5)
Cannula ED (%)	74.7 (3.0)	69.3 (4.2)	71.4 (1.9)
NMT (%)	6.9 (2.0)	8.9 (3.1)	6.2 (2.1)
Filter Delivery (%)	61.6 (4.8)	53.4 (6.2)	55.3 (4.1)
Recovery (%)*	93.8 (0.7)	92.9 (1.2)	90.2 (0.3)**

Values are reported as a percentage of nominal dose loaded into the capsule. Standard deviations (SD) shown in parenthesis [n = 3]

*p < 0.05 significant effect of system design on Recovery (one-way ANOVA)

**p < 0.05 significant difference compared to Steady State (post-hoc Tukey)

Table V Mean (SD) *In Vitro* Aerosol Drug Delivery Using the Aerogen Solo Nebulizer with Passive Nasal Inhalation Conditions and 8 LPM System Flow Rate

Description	Passive nasal
ED (mg)	2.8 (0.1)
Device (%)	1.7 (0.9)
Tee (%)	52.6 (3.3)
Tubing (%)	29.9 (0.2)
Cannula ED (%)	15.7 (3.8)
NMT (%)	0.0 (0.0)
Filter Delivery (%)	1.4 (0.2)
Recovery (%)	85.7 (4.0)

Values are reported as a percentage of ED. Standard deviations (SD) shown in parenthesis [n = 3]

A significant advantage of the system was very rapid actuation of the device, requiring 0.2 s to depress the air syringe, which made it relatively easy to synchronize delivery with inhalation. As a result, exhalation losses were very small. Comparison of steady state and cyclic nasal conditions in Table IV indicates that exhalation losses were likely in the range of 5% of the loaded dose, which can be considered minimal in this system. Minimizing exhalation losses clearly helps to improve lung delivery efficiency. Furthermore, many inhaled medications pose a risk to caregivers and others through unintended environmental exposure arising from exhalation losses, or aerosol that otherwise escapes from the delivery system. The minimal exhalation losses of the LV-DPI system therefore provides an advantage over other aerosol delivery systems with high exhalation and environmental losses.

Performance of the mesh nebulizer setup in this study was similar to other nasal cannula interface systems including the *in vitro* study of Perry *et al.* (17) and the *in vivo* studies of Dugernier *et al.* (36) and Zeman *et al.* (37). The mesh nebulizer delivery efficiency to the tracheal filter was 1.4% of the nebulized dose and required 90 s to delivery 0.039 mg of drug to the lungs during passive breathing. In contrast, the optimized LV-DPI system during passive respiration delivered approximately 55% of the loaded dose to the tracheal filter, representing a 40-fold increase in delivery efficiency. Considering delivery time, the optimized LV-DPI system delivered 1.7 mg of the model active medication (AS) to the filter over 5 actuations requiring approximately 25 s under passive breathing conditions (5 breaths requiring 5 s each). For comparison, the mesh nebulizer would have to run approximately 1.1 h to deliver this amount of drug to the filter, representing an approximate 150-fold increase in delivery time.

Few studies have attempted the delivery of a powder aerosol through a nasal cannula interface. The most relevant study performed outside of our group is likely Okuda *et al.* (12), who

considered a spray dried mannitol formulation delivered during high flow nasal cannula (HFNC) conditions through an adult nasal cast model. Under best case conditions, the maximum dose delivered to a tracheal filter was approximately 20% of the loaded dose. While filter delivered dose was higher in the current study than with Okuda *et al.* (12), a few differences should be noted. First, Okuda *et al.* (12) consider HFNC therapy, where flow rates are typically higher (15 to 40 L/min) compared with 8 to 11 L/min in the current study. To accommodate these higher flow rates, HFNC systems typically employ larger diameter tubing (~10 mm ID) and larger bore nasal cannula. Finally, the study of Okuda *et al.* (12) implemented the humidified gas of the HFNC system to aerosolize the powder, which created a simpler system setup but prevented coordination with inhalation.

Considering previous work from our group, the study of Longest *et al.* (19) evaluated powder aerosol delivery during LFNC therapy. A similar spray dried AS EEG formulation was continually aerosolized using a 3D rod array inline DPI without the inclusion of a nasal model and cyclic respiration. For the best-case design developed in Longest *et al.* (19), the cannula ED was 61% of the loaded dose. For a consistent comparison, the steady state cannula ED in the current study was 75%, indicating a reasonable improvement with the LV-DPI device. However, the most significant advantage of the LV-DPI device may be the rapid actuation time of 0.2 s and short dose delivery period out of the cannula of 0.7 s post initial actuation. In contrast, the 3D rod array device in the study of Longest *et al.* (19) was actuated with the continuously flowing LFNC gas, which prevented synchronization with inhalation. Additional advantages of the LV-DPI compared with the 3D rod array inline device include a combination of the close and pierce steps and actuation with very small volumes of air (~10 ml).

In this study, AS was implemented as a model drug that is relatively safe and inexpensive with well-established quantification methods. However, the LV-DPI system is intended to deliver a variety of medications that require high powder doses. Specific examples of envisioned applications include inhaled antibiotics, osmotic agents, surfactants and anti-inflammatory medications. In transitioning to other formulations, maintaining a highly dispersible powder will be a key requirement. In previous work, we have demonstrated that highly dispersible EEG formulations can be made with terbutaline sulfate (38) and ciprofloxacin (8,11,39). The development of spray dried EEG surfactant formulations is also in progress (40,41). The previous study of Son *et al.* (35) demonstrated that L-leucine was important to maintain good powder dispersion of the spray dried formulation. For hygroscopic growth, it is also important that the hygroscopic excipient remain accessible to the external environment surrounding the initial particle. In addition to Son *et al.* (35), further work is needed to better understand the relationship between spray dried EEG powder properties and aerosol formation.

Limitations for this study include the need for multiple NMT models to study performance variability in different patients, an observed variability in reproducing the exact position/angle of the nasal cannula in the nose, the use of hard plastic for the Y-connector and cannula instead of flexible materials, and the use of a filter placed at the end of the trachea to approximate lung dose. Since variability exists between subjects, using one model does not take into account physiological differences that will be encountered during future clinical use with this system. In addition to intersubject variability, intrasubject variability in cannula positioning may also have an effect on the delivery performance. Exhalation losses with this system are also difficult to quantify and may be underestimated, as the filter captures the particles and prevents them from being exhaled. Exhalation losses in this study refers to aerosol that is held in the nose and nasopharynx region and then exhaled, as well as aerosol that never enters the nose due to a flow mismatch between the cannula velocity and nostril inhalation velocity. It is noted that exhalation losses from the lungs will be minimized due to the use of EEG formulations. These formulations are intended to have small initial aerosol diameters to maximize lung penetration. Inclusion of the hygroscopic excipient fosters droplet size increase within the lungs thereby maximizing deposition and potentially targeting drug delivery to different lung regions (8,42–45).

CONCLUSIONS

In conclusion, the LV-DPI device together with modified system components was shown to provide high efficiency aerosol delivery through a NMT model and to a tracheal filter. Very rapid dose delivery with a small volume of air facilitated synchronization with inspiratory flow during cyclic breathing. Lung delivery efficiency was near 60% of the loaded powder mass. For aerosol administration during LFNC therapy, delivery performance was improved compared with a previously developed 3D rod array inline DPI. Compared with a mesh nebulizer, lung delivery efficiency was 40 times greater and dose delivery rate was 150 times faster. These dose delivery efficiencies and times can be further improved in systems developed exclusively for pharmaceutical aerosol administration without the limitations associated with simultaneous LFNC gas delivery.

ACKNOWLEDGMENTS AND DISCLOSURES

Research reported in this publication was supported by the Eunice Kennedy Shriver National Institute of Child Health & Human Development of the National Institutes of Health under Award Number R01HD087339 and by the National Heart, Lung and Blood Institute of the National Institutes of Health under Award Number R01HL139673. The content is

solely the responsibility of the authors and does not necessarily represent the official views of the National Institutes of Health. Virginia Commonwealth University is currently pursuing patent protection of EEG aerosol delivery, DPI aerosol generation devices and patient interfaces, which if licensed, may provide a future financial interest to the authors.

ABBREVIATIONS

3D	Three dimensional
AS	Albuterol sulfate
ASL	Active servo lung
CFD	Computational fluid dynamics
DPI	Dry powder inhaler
ED	Emitted dose
EEG	Excipient enhanced growth
FPF	Fine particle fraction
HFNC	High flow nasal cannula
HPLC	High performance liquid chromatography
HPMC	Hydroxypropyl methylcellulose
LFNC	Low flow nasal cannula
LPM	Liters per minute
LV	Low volume
MMAD	Mass median aerodynamic diameters
N2L	Nose-to-lung
NGI	Next Generation Impactor
NMT	Nose-mouth-throat
SL	Streamlined

REFERENCES

1. Behara SRB, Longest PW, Farkas DR, Hindle M. Development of high efficiency ventilation bag actuated dry powder inhalers. Int J Pharm. 2014;465:52–62.
2. Pornputtapitak W, El-Gendy N, Mermis J, O'Brein-Ladner A, Berkland C. NanoCluster budesondie formulations enable efficient drug delivery driven by mechanical ventilation. Int J Pharm. 2014;462:19–28.
3. Tang P, Chan HK, Rajbhandari D, Phipps P. Method to introduce mannitol powder to intubated patients to improve sputum clearance. J Aerosol Med Pulm Drug Deliv. 2011;24:1–9.
4. Laube BL, Sharpless G, Shermer C, Sullivan V, Powell K. Deposition of dry powder generated by solovent in Sophia anatomical infant nose-throat (SAINT) model. Aerosol Sci Technol. 2012;46:514–20.
5. Farkas D, Hindle M, Longest PW. Application of an inline dry powder inhaler to deliver high dose pharmaceutical aerosols during low flow nasal cannula therapy. Int J Pharm. 2018;546:1–9.
6. Farkas D, Hindle M, Longest PW. Development of an Inline Dry Powder Inhaler That Requires Low Air Volume. J Aerosol Med Pulm Drug Deliv. 2018;31:255–65
7. Feng B, Tang P, Leung SSY, Dhanani J, Chan H-K. A novel in-line delivery system to administer dry powder mannitol to mechanically ventilated patients. J Aerosol Med Pulm Drug Deliv. 2017;30:100–7.
8. Longest PW, Golshahi L, Behara SRB, Tian G, Farkas DR, Hindle M. Efficient nose-to-lung (N2L) aerosol delivery with a dry powder inhaler. J Aerosol Med Pulm Drug Deliv. 2015;28:189–201.
9. Morley CJ, Miller CW, Bangham AD, Davis JA. Dry artificial lung surfactant and its effect on very premature babies. Lancet. 1981;317:64–8.
10. Everard ML, Devadason SG, LeSouef PN. In vitro assessment of drug delivery through an endotracheal tube using a dry powder inhaler delivery system. Thorax. 1996;51:75–7.
11. Walenga RL, Longest PW, Kaviratna A, Hindle M. Aerosol drug delivery during noninvasive positive pressure ventilation: effects of intersubject variability and excipient enhanced growth. J Aerosol Med Pulm Drug Deliv. 2017;30:190–205.
12. Okuda T, Tang P, Yu J, Finlay WH, Chan H-K. Powder aerosol delivery through nasal high-flow system: in vitro feasibility and influence of process conditions. Int J Pharm. 2017;533:187–97.
13. Ward JJ. High-flow oxygen administration by nasal cannula for adult and perinatal patients. Respir Care. 2013;58:98–120.
14. Hess DR. The mask of noninvasive ventilation: principles of design and effects on aerosol delivery. J Aerosol Med. 2007;20:S85–99.
15. Bhashyam AR, Wolf MT, Marcinkowski AL, Saville A, Thomas K, Carcillo JA, *et al*. Aerosol delivery through nasal cannulas: an in vitro study. J Aerosol Med Pulm Drug Deliv. 2008;21:181–7.
16. Dhand R. Aerosol therapy in patients receiving noninvasive positive pressure ventilation. J Aerosol Med Pulm Drug Deliv. 2012;25:63–78.
17. Perry SA, Kesser KC, Geller DE, Selhorst DM, Rendle JK, Hertzog JH. Influences of cannula size and flow rate on aerosol drug delivery through the Vapotherm humidified high-flow nasal cannula system. Pediatr Crit Care Med. 2013;14:E250–6.
18. Sunbul F, Fink JB, Harwood R, Sheard MM, Zimmerman RD, Ari A. Comparison of HFNC, bubble CPAP and SiPAP on aerosol delviery in neonates: An in-vitro study. *Pediatr Pulmonol*. 2014; https://doi.org/10.1002/ppul.23123.
19. Longest PW, Behara SRB, Farkas DF, and Hindle M. Efficient generation and delivery of dry powder aeorsols during low flow oxygen administration. *Drug Delivery to the Lungs - DDL 24*. 2014; http://ddl-conference.com/files/DDL24Abstracts/oral/05.Hindle.pdf
20. Longest PW, Golshahi L, Hindle M. Improving pharmaceutical aerosol delivery during noninvasive ventilation: effects of streamlined components. Ann Biomed Eng. 2013;41:1217–32.
21. Longest PW, Tian G, Hindle M. Improving the lung delivery of nasally administered aerosols during noninvasive ventilation - An application of enhanced condensational growth (ECG). *J Aerosol Med Pulm Drug Deliv*. 2011;24:103–18. https://doi.org/10.1089/jamp.2010.0849.
22. Longest PW, Azimi M, Golshahi L, Hindle M. Improving aerosol drug delivery during invasive mechanical ventilation with redesigned components. Respir Care. 2014;59:686–98.

23. Behara SRB, Farkas DR, Hindle M, Longest PW. Development of a high efficiency dry powder inhaler: effects of capsule chamber design and inhaler surface modifications. Pharm Res. 2014;31: 360–72.
24. Golshahi L, Tian G, Azimi M, Son Y-J, Walenga RL, Longest PW, *et al.* The use of condensational growth methods for efficient drug delivery to the lungs during noninvasive ventilation high flow therapy. Pharm Res. 2013;30:2917–30.
25. Guilmette RA, Wicks JD, Wolff RK. Morphometry of human nasal airways in vivo using magnetic resonance imaging. J Aerosol Med. 1989;2:365–77.
26. Kelly JT, Asgharian B, Kimbell JS, Wong B. Particle deposition in human nasal airway replicas manufactured by different methods. Part I: inertial regime particles. Aerosol Sci Technol. 2004;38: 1063–71.
27. Kelly JT, Asgharian B, Kimbell JS, Wong B. Particle deposition in human nasal airway replicas manufactured by different methods. Part II: ultrafine particles. Aerosol Sci Technol. 2004;38:1072–9.
28. Kimbell JS, Segal RA, Asgharian B, Wong BA, Schroeter JD, Southall JP, *et al.* Characterization of deposition from nasal spray devices using a computational fluid dynamics model of the human nasal passages. J Aerosol Med.-Depos Clear Eff Lung. 2007;20:59–74.
29. Schroeter JD, Kimbell JS, Asgharian B. Analysis of particle deposition in the turbinate and olfactory regions using a human nasal computational fluid dynamics model. J Aerosol Med. 2006;19:301–13.
30. Xi J, Longest PW. Numerical predictions of submicrometer aerosol deposition in the nasal cavity using a novel drift flux approach. Int J Heat Mass Transf. 2008;51:5562–77.
31. Xi J, Longest PW. Characterization of submicrometer aerosol deposition in extrathoracic airways during nasal exhalation. Aerosol Sci Technol. 2009;43:808–27.
32. Xi J, Longest PW. Transport and deposition of micro-aerosols in realistic and simplified models of the oral airway. Ann Biomed Eng. 2007;35:560–81.
33. ICRP. Human respiratory tract model for radiological protection. New York: Elsevier Science Ltd.; 1994.
34. Franca EET, de Andrade AFD, Cabral G, Almeida P, Silva KC, Galindo VC, *et al.* Nebulization associated with bi-level noninvasive ventilation: analysis of pulmonary radioaerosol deposition. Respir Med. 2006;100:721–8.
35. Son Y-J, Longest PW, Hindle M. Aerosolization characteristics of dry powder inhaler formulations for the excipient enhanced growth (EEG) application: effect of spray drying process conditions on aerosol performance. Int J Pharm. 2013;443:137–45.
36. Dugernier J, Hesse M, Jumetz T, Bialais E, Roeseler J, Depoortere V, *et al.* Aerosol delivery with two nebulizers through high-flow nasal cannula: a randomized cross-over single-photon emission computed tomography-computed tomography study. Journal of Aerosol Medicine and Pulmonary Drug Delivery. 2017;30:349–58.
37. Zeman KL, Rojas Balcazar J, Fuller F, Donn KH, Boucher RC, Bennett WD, *et al.* A trans-nasal aerosol delivery device for efficient pulmonary deposition. J Aerosol Med Pulm Drug Deliv. 2017;30: 223–9.
38. Behara SRB, Longest PW, Farkas DR, Hindle M. Development and comparison of new high-efficiency dry powder inhalers for carrier-free formulations. J Pharm Sci. 2014;103:465–77.
39. Farkas DR, Hindle M, Longest PW. Characterization of a new high-dose dry powder inhaler (DPI) based on a fluidized bed design. Ann Biomed Eng. 2015;43:2804–15.
40. Boc ST, Farkas DR, Longest PW, Hindle M. Spray dried pulmonary surfactant powder formulations: Development and characterization. *Respiratory Drug Delivery*. 2018;2:635–8.
41. Boc ST, Farkas DR, Longest PW, Hindle M. Aerosolization of spray dried pulmonary surfactant powder using a novel low air volume actuated dry powder inhaler. Respiratory Drug Delivery. 2018;2:639–42.
42. Longest PW, Hindle M. Numerical model to characterize the size increase of combination drug and hygroscopic excipient nanoparticle aerosols. Aerosol Sci Technol. 2011;45:884–99.
43. Tian G, Hindle M, Longest PW. Targeted lung delivery of nasally administered aerosols. Aerosol Sci Technol. 2014;48:434–49.
44. Tian G, Longest PW, Li X, Hindle M. Targeting aerosol deposition to and within the lung airways using excipient enhanced growth. J Aerosol Med Pulm Drug Deliv. 2013;26:248–65.
45. Hindle M, Longest PW. Condensational growth of combination drug-excipient submicrometer particles for targeted high-efficiency pulmonary delivery: evaluation of formulation and delivery device. J Pharm Pharmacol. 2012;64:1254–63.